Article

Investigation into Influences of Hydraulic Fracturing for Hard Rock Weakening in Underground Mines

Xu Cao [1], Saisai Wu [2],* and Qingyuan He [3]

1   Shaanxi Bureau of State Mine Safety Supervision Bureau, Xi'an 710001, China
2   Shaanxi Key Laboratory of Geotechnical and Underground Space Engineering, School of Resources Engineering, Xi'an University of Architecture and Technology, Xi'an 710055, China
3   State Key Laboratory of Coal Resources and Safe Mining, School of Mines, China University of Mining and Technology, Xuzhou 221116, China
*   Correspondence: saisai.wu@xauat.edu.cn

Abstract: The long overhanging distance of hard roofs and long-collapse steps induces a large area of suspension on the working face in underground coal mines, resulting in excessive pressure and deformation on the surrounding rocks of the adjacent roadway in the work face, which seriously threatens the safety of coal mining operations. In this study, in order to study the hydraulic fracturing effects on hard roofs, numerical simulation and in situ tests were conducted. The analysis and comparison of fracturing effects under different hydraulic fracturing parameters were carried out, and the reasonable hydraulic fracturing parameters of the hydraulic weakening of hard roofs were designed accordingly. Based on designed hydraulic fracturing, industrial tests were conducted in the field while stress and deformation were recorded. The results show that hydraulic fracturing could effectively reduce the pressure of the hard roof. Hydraulic fracturing effectively destroyed the cantilever beam structure above the coal pillar, reduced the stress concentration, and moderated mineral pressure at the working face. The proposed methods and obtained results provide theoretical and technical support for the treatment of underground mines with hard roofs.

Keywords: hydraulic fracturing; hard roofs; mining pressure; numerical simulation

1. Introduction

Currently, over 40% of fully mechanized mining faces in underground coal mines in China experience significant problems with hard roof pressure, especially those with extremely thin direct roofs [1,2]. How to effectively control the hard roof over the working face has become the focus of current research. If the hard roof cannot naturally collapse from above the working face, large areas of suspension on the working face occur, resulting in excessive roof pressure on hydraulic support systems [3,4]. In addition, if large areas of the suspended roof collapse due to roof cutting, severe impact loads would be generated, seriously threatening the safety of coal mining operations [5–7]. Hydraulic fracturing is a safe and efficient method for cutting hard rock layers, and its application range is constantly expanding [8–11]. By injecting high-pressure water into the hard roof, cracks appear in the hard roof and expand, thus changing the structure of the rock layers [12]. After fracturing treatment, multi-level water pressure cracks and secondary cracks appear inside the hard roof, which damage the structural integrity of the rock, weaken its overall strength, and ultimately achieve the goal of reducing pressure [13,14]. The core research content of hydraulic fracturing technology is the fracturing mechanism, which mainly includes crack initiation and crack extension.

Hubbert [15] found that regardless of the permeability of the fracturing fluid, the direction of fracture propagation on the fracturing surface always remained perpendicular to the direction of the minimum principal stress. This conclusion provides an important basis for further research on hydraulic fracturing technology. In areas affected by geological

structural stress, especially near the faults, the minimum principal stress is usually in the horizontal direction. In the geological structure compression area, the minimum principal stress is in the vertical direction, and the hydraulic fracturing surface extends horizontally. Griffith [16] described that when the release rate of strain energy increases to a certain extent, cracks experience unstable failure and propagation. When the elastic strain of cracks exceeds the tensile strength of the material, it continuously expands until it reaches a critical value. According to the theory proposed by Palaniswamy [17], cracks usually develop in a direction that generates higher strain energy release rates. Once the predetermined energy level is reached, cracks rapidly expand. Fan. et al. [18] proposed a calculation model based on the tensile strength criterion, which can effectively predict the development of hydraulic fractures. By analyzing the level of geostress and the orientation of the wellhead, this model can accurately predict the hydraulic fracturing pressure and the formation and expansion degree of fractures.

Extensive research has been conducted in the area of hydraulic fracturing mechanisms [19–23]. Deng et al. [24] studied the entire hydraulic failure process, including hydraulic fracture initiation and crack propagation through true triaxial testing and a finite element numerical simulation. The effects of the groove angle, length, and injection flow rate of fracturing fluid on directional hydraulic cracks were studied. By analyzing uneven forces, the formation and development of cracks were predicted. Ham et al. [25,26] studied and explored the propagation of hydraulic cracks in elastic and ductile media, with a focus on the geometric shape of hydraulic cracks under different fracturing times. The real-time monitoring of hydraulic crack propagation behavior in two-dimensional confined gelatin samples was conducted by changing the stiffness of the gelatin, the viscosity of the fracturing fluid, and flow rates. He et al. [27] studied the interaction between natural cracks and horizontal radial hydraulic cracks through theoretical analysis and numerical simulation methods. The results showed that the inclination angle, approach angle, and triaxial stress of natural cracks all affect the propagation of hydraulic cracks. The aforementioned studies mainly focused on the hydraulic fracturing mechanism through laboratory tests, rarely examining the effects of hydraulic fracturing through in situ tests.

In this study, the hydraulic fracturing parameters for hard roof weakening were studied through laboratory experiments, theoretical analysis, numerical simulation, and in situ industrial experiments. The effects of hydraulic fracturing parameters, including fracturing intervals, water injection pressures, and borehole spacing on hard roof weakening, were examined. To verify the effectiveness of the design parameters, the roadway displacement and pressure before and after hydraulic fracturing were recorded and compared. The results showed that hydraulic fracturing treatment redistributed and reduced the stress of the roadway surrounding the rock and eliminated the stress concentration caused by the large areas of suspension on the working face, thus achieving effective control of roadway deformation. The proposed methods and obtained results provided theoretical and technical support for effectively controlling hard roof pressure in fully mechanized mining faces.

2. Numerical and In Situ Testing Programs

To investigate hydraulic fracturing weakening technology for hard roofs in underground coal mines, one of the coal mines that experienced hard roof issues in Shannxi province was selected for numerical simulation and in situ tests. Different layers, including the sandy mudstone and medium-grained sandstone, were observed on the strata, but only the harder medium-grained sandstone layer was investigated for hydraulic fracturing. For the examination of the mechanical parameters of the hard roof, a relatively intact portion of the drilled rock cores was selected for the preparation of specimens. Three different sizes of specimens were prepared for uniaxial compression tests, rock shear tests, and Brazilian splitting tests. The physical and mechanical parameters of the hard roof rock layer are displayed in Table 1. The experimental results show that the hard roof of the working face belongs to a hard roof. The tensile strength of the hard roof of the medium sandstone in the

working face is 7.8 MPa, with a uniaxial compressive strength of 71.3 MPa, elastic modulus of 46.4 MPa, cohesive force of 9.1 MPa, and internal friction angle of 38°.

Table 1. The physical and mechanical parameters of the hard roof rock layer.

Parameters	Density (g·cm^{-3})	Tensile Strength (MPa)	Uniaxial Compressive Strength (MPa)	Elastic Modulus (GPa)	Cohesion (MPa)	Internal Friction Angle (°)
Sandstone	2.83	7.8	71.3	46.4	9.1	38

2.1. Numerical Simulation Methods

Based on the physical and mechanical parameters of the hard rock layer, a physical and mechanical parameter model of medium-grained sandstone was established using FLAC3D-6.0 numerical simulation software. The reasons behind using the FLAC3D-6.0 numerical simulation software are that it can achieve the analysis of thermal fluid–solid coupling in the hydraulic fracturing of the roof, as well as obtain the crack propagation law under cutting groove conditions. A numerical model of medium-grained sandstone with dimensions of 21 m, 7 m, and 30 m in length, width, and height is shown in Figure 1a. For the boundary condition of numerical simulation, the upper and lower boundaries and surrounding boundaries of the model are set as fully constrained type boundaries, and the Mohr–Coulomb constitutive model is selected for numerical calculation. The mechanical properties of the rock mass in numerical simulation are set based on the experimental results of the hard roof rock layer (Table 1). The spacing between fracturing segments in hydraulic fracturing boreholes is one of the important factors affecting the effectiveness of hydraulic fracturing. To investigate the impacts of the different spacing of hydraulic fracturing segments on hydraulic fracturing, numerical simulations were conducted under three different spacing conditions of boreholes at 1.1 m, 2.2 m, and 3.3 m (Figure 1b). The hydraulic fracturing boreholes were drilled at the center of the model at an angle of 70° to the horizontal direction, with a diameter and depth of 56 mm and 20 m, respectively.
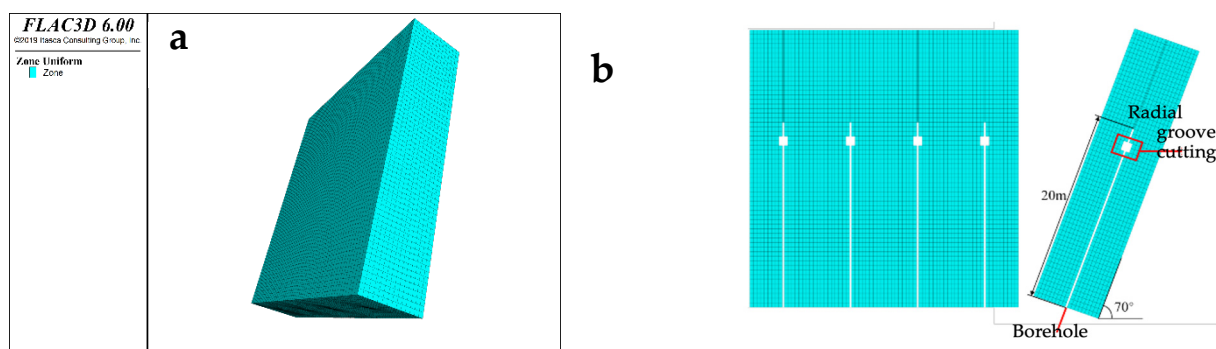
Figure 1. Numerical model of working face: (**a**) hard roof of working face; (**b**) layout diagram of hydraulic fracturing boreholes.

2.2. In Situ Testing Methods

Based on numerical model results, one of the coal mines that experienced the hard roof issues in Shannxi Province was selected for in situ tests. Hydraulic fracturing boreholes were arranged on the side of the coal body towards the working face on the side of the return airway, with the drilling direction opposite to the advancing direction. The ZDY1200LP-tracked drilling rig was used on the coal mine site to complete the drilling operation. The front end of the working oil cylinder was equipped with a bidirectional hydraulic locking device, which could ensure stable drilling. Additionally, this drilling rig could stably drill according to the preset inclination angle, azimuth angle, and length of the borehole. The spacing of the hydraulic fracturing boreholes is 7.0 m, and the angle

between the boreholes and the roof of the roadway is 70° (Figure 2). The diameter of the borehole is 56 mm, and the depth of the inclined borehole is 21.6 m. The inclined depth of the hydraulic fracturing borehole in the coal seam section is 3.9 m, with 17.7 m in the rock layer. The reverse fracturing method for the hydraulic fracturing borehole was used, which started from 1.3 m at the bottom of the borehole and radially towards the end of borehole at intervals of 2.2 m. To accurately evaluate the fracturing effect of the hard roof of the working face, the real-time monitoring of the water injection pressure, water volume, and water injection time of hydraulic fracturing was carried out throughout the entire process. Real-time monitoring of the water output from adjacent hydraulic fracturing boreholes or the anchor rod and cable boreholes was also carried out throughout the entire process. If injected water was immersed from adjacent hydraulic fracturing boreholes that produced water, the fracture network formed by hydraulic fracturing had been connected in the basic top, which indicated the hydraulic fracturing results were good. After the hydraulic fracturing was completed, the inside conditions of the hydraulic fracturing boreholes were observed using a borehole peeper. By observing the crack development and shape inside the hydraulic fracturing boreholes, the crack development and expansion range of cracks were analyzed.
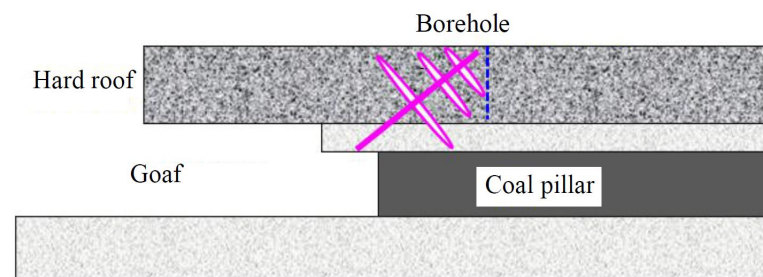
Figure 2. Schematic diagram of hydraulic fracturing effects.

3. Numerical Simulation Results

3.1. Different Fracturing Intervals

The failure situation and stress distribution of the surrounding rock in the hydraulic fracturing borehole in the working face under different fracturing interval conditions are shown in Figure 3. In the figures of fracture conditions, the blue areas represent the occurrence of shear failure, the pink areas represent the combination of shear and tension failure, and the olive area represents the occurrence of tension failure. In the figures of stress conditions, the color from blue to red caused an increase in the stress concentrations. From Figure 3, it can be seen that as the spacing between fracturing intervals in the borehole increased, the spacing of the fracture network formed between adjacent fracturing sections also increased. At the fracturing intervals between the boreholes at 1.1 m, the hard roof rock between the two fracturing sections was subjected to repeated fracturing. The cracks formed between the two fracturing sections were too close, which affected the generation of cracks in the next fracturing section. At fracturing intervals of 2.2 m, the fracture network that formed between the two fracturing sections was independent of each other and was conducive to the generation of fractures in the next fracturing section. At fracturing intervals of 3.3 m, the distance between the fracture networks formed between the two fracturing sections further increased, and the fracture networks that formed between the two fracturing sections were independent and did not interfere with each other. However, there was a large unfractured zone between the fracturing sections, and the number of fractures that could be performed within the drilling depth was reduced.

Comparing the simulation results of different fracturing interval spacing, it could be concluded that a reasonable fracturing interval was one of the key parameters determining the hydraulic fracturing effects. If the spacing between fracturing sections is too large, the cracks generated by adjacent fracturing sections are independent of each other and cannot form a continuous fracturing transformation zone. If the spacing between fracturing sec-

tions is too small, although the fracture network generated by fracturing is continuous and the weakening effect is good, an overlap in the fracturing area is produced, which affects the formation of new fractures and significantly reduces the efficiency of the fracturing construction. Therefore, based on numerical simulation results and the in situ situation of the working face, a reasonable spacing of 2.2 m between fracturing sections can be determined, which can fully fracture the surrounding rock between the fracturing sections.

(**a**) Fracture conditions at interval of 1.1 m   (**b**) Stress conditions at interval of 1.1 m

(**c**) Fracture conditions at interval of 2.2 m   (**d**) Stress conditions at interval of 2.2 m

(**e**) Fracture conditions at interval of 3.3 m   (**f**) Stress conditions at interval of 3.3 m
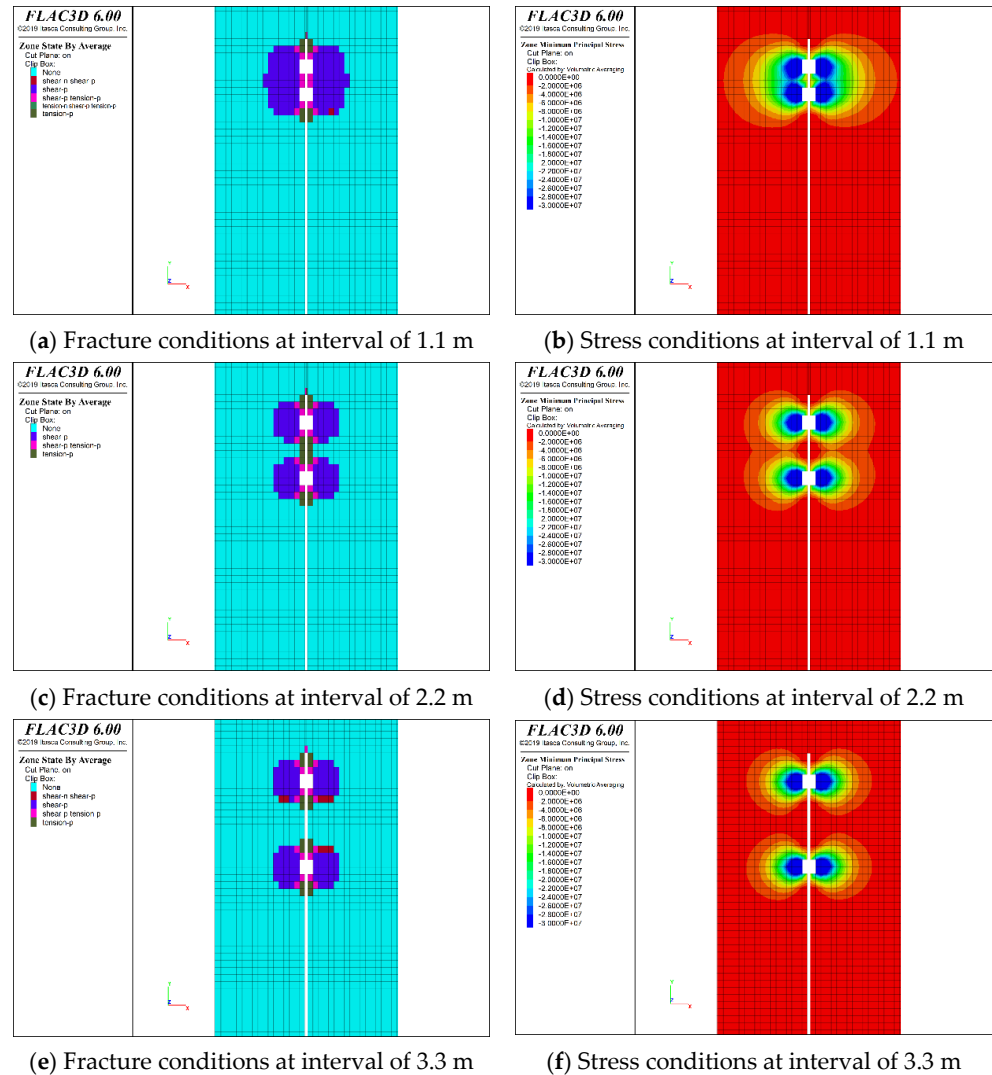
Figure 3. Simulation results of fracturing effect under different fracturing interval conditions.

3.2. Different Water Injection Pressures

The failure and stress distribution of the surrounding rock in the hydraulic fracturing borehole at the working face under different water injection pressure conditions are shown in Figure 4. As shown in Figure 4, with the increase in the water injection pressure, the degree of rock damage to both sides of the hydraulic fracturing borehole gradually increased, and the range of damage also significantly increased. At a water injection pressure of 20 MPa, the degree of damage and development of fractures in the surrounding rock of hydraulic fracture drilling was relatively small. When the water injection pressure increased to 25 MPa, the degree of damage to the surrounding rock and the degree of crack development was enhanced while the range of the crack network was expanded. At a water injection pressure of 30 MPa, the surrounding rock of the basic top hydraulic fracturing borehole was fully damaged, and the degree of crack network development was good, showing good fracturing effects. A reasonable injection pressure is one of

the key parameters determining the effectiveness of hydraulic fracturing. If the water injection pressure is too small, the degree of damage to the surrounding rock and the range of crack expansion in the hydraulic fracturing boreholes becomes very limited, and adjacent hydraulic fracturing boreholes find it difficult to form a continuous crack network. Therefore, based on numerical simulation results and the in situ situation of the working face, a reasonable water injection pressure of 30 MPa was determined to fully fracture the surrounding rock between the fracturing sections.

(**a**) Fracture conditions at pressure of 20 MPa (**b**) Stress conditions at pressure of 20 MPa

(**c**) Fracture conditions at pressure of 25 MPa (**d**) Stress conditions at pressure of 25 MPa

(**e**) Fracture conditions at pressure of 30 MPa (**f**) Stress conditions at pressure of 30 MPa
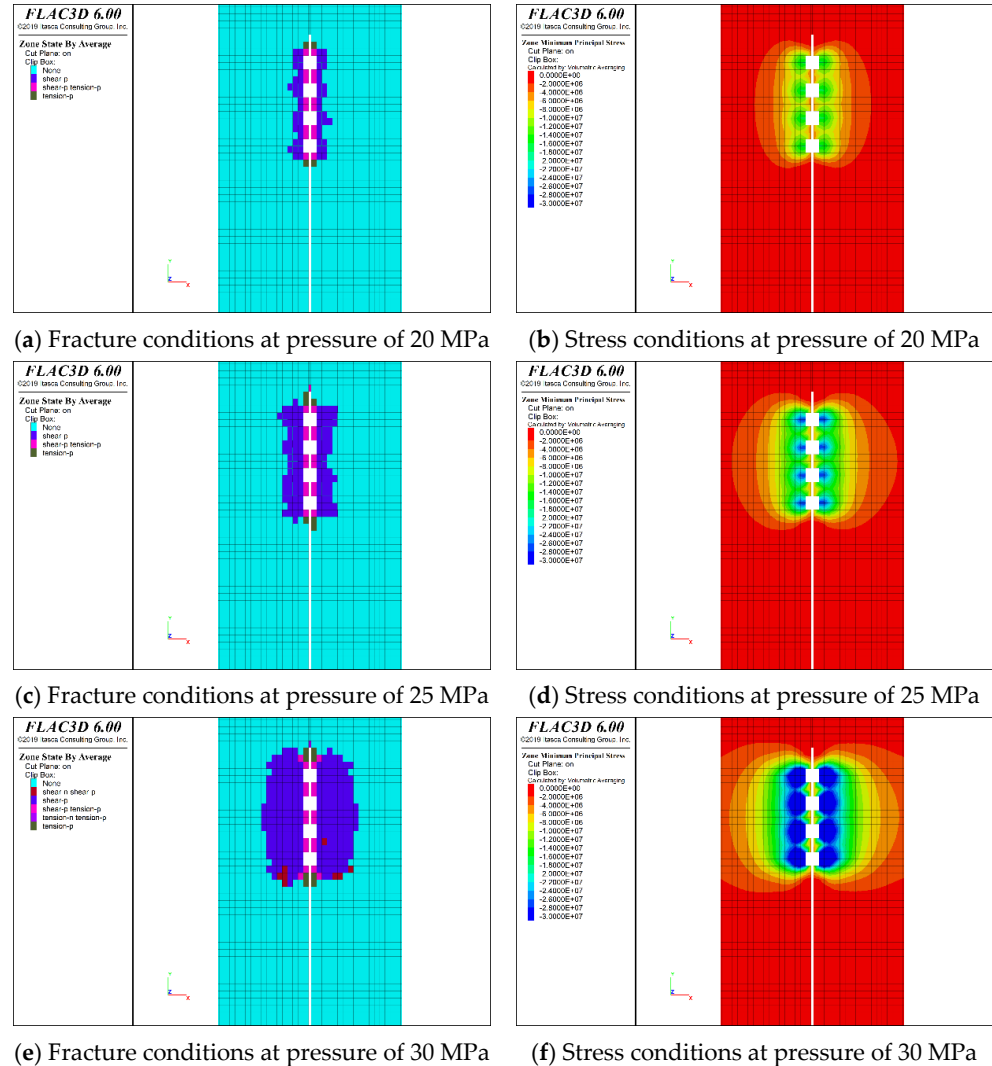
Figure 4. Simulation results of fracturing effect under different water injection pressures.

3.3. Different Borehole Spaces

The failure and stress distribution of the surrounding rock in hydraulic fracturing and drilling in the working face under different levels of borehole spacing are shown in Figure 5. From Figure 5, it can be seen that as the spacing between boreholes increases, the degree of the surrounding rock damage between adjacent hydraulic fracturing boreholes gradually weakens. At a spacing of 7 m between the boreholes, the hard roof rock between adjacent hydraulic fracturing boreholes was fully damaged, and the cracks formed between the two boreholes were well connected. When the spacing between the boreholes increased to 14 m and 21 m, the degree of damage and crack development in the surrounding rock between the adjacent hydraulic fracturing boreholes weakened. The cracks did not penetrate, and a large unfractured area between the two fracturing boreholes was observed. If the spacing between boreholes is too large, the cracks generated by adjacent hydraulic fracturing

boreholes cannot develop and penetrate. If the spacing between boreholes is too small, although the fracture network generated by each hole during fracturing is continuous and the surrounding rock damage effect is good, the construction efficiency is reduced. Therefore, based on numerical simulation results and the in situ situation of the working face, a reasonable drilling spacing of 7 m was determined, which could fully fracture the surrounding rock between adjacent hydraulic fracturing boreholes.

(**a**) Fracture condition at spacing of 21 m

(**b**) Stress conditions at spacing of 21 m

(**c**) Fracture conditions at spacing of 14 m

(**d**) Stress conditions at spacing of 14 m

(**e**) Fracture conditions at spacing of 7 m

(**f**) Stress conditions at spacing of 7 m
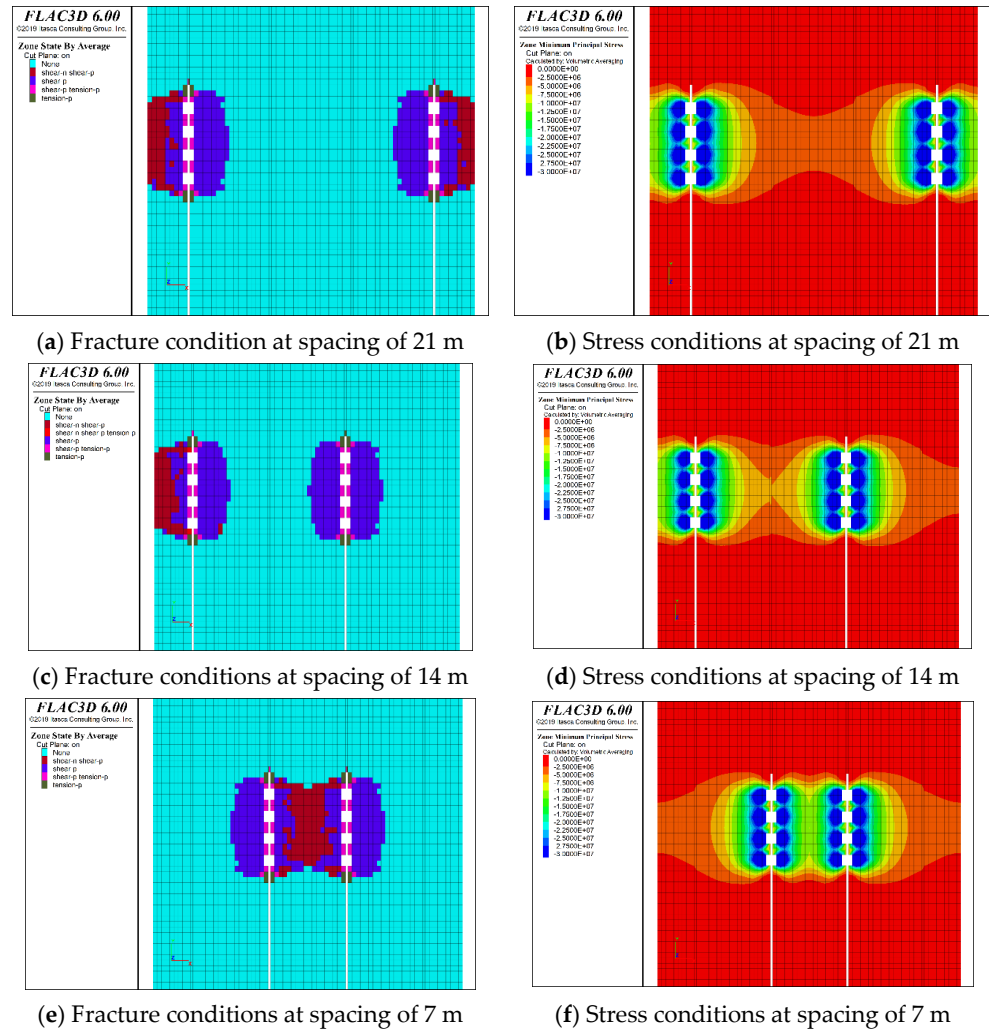
Figure 5. Simulation results of fracturing effect under different borehole spacing conditions.

3.4. Hydraulic Fracturing Parameters

Based on the numerical simulation results, the recommended hydraulic fracturing parameters for the working face are shown in Table 2. Based on the hydraulic fracturing parameters, the surrounding rock failure effect during the hydraulic fracturing process of the hard roof was simulated (Figure 6). From Figure 6, it can be seen that the hard roof rock between hydraulic fracturing boreholes in the model was fully damaged, and these fractures were well connected to form well-developed fracture networks. Therefore, the designed hydraulic fracturing parameters were sufficient to damage the surrounding rock with a well-developed fracture network and a large range of surrounding rock damage.

Table 2. Reasonable hydraulic fracturing parameters.

Parameters	Designed Values
Fracturing intervals	2.2 m
Water injection pressures	30 MPa
Borehole spacing	7 m

(**a**) Fracture condition

(**b**) Stress conditions
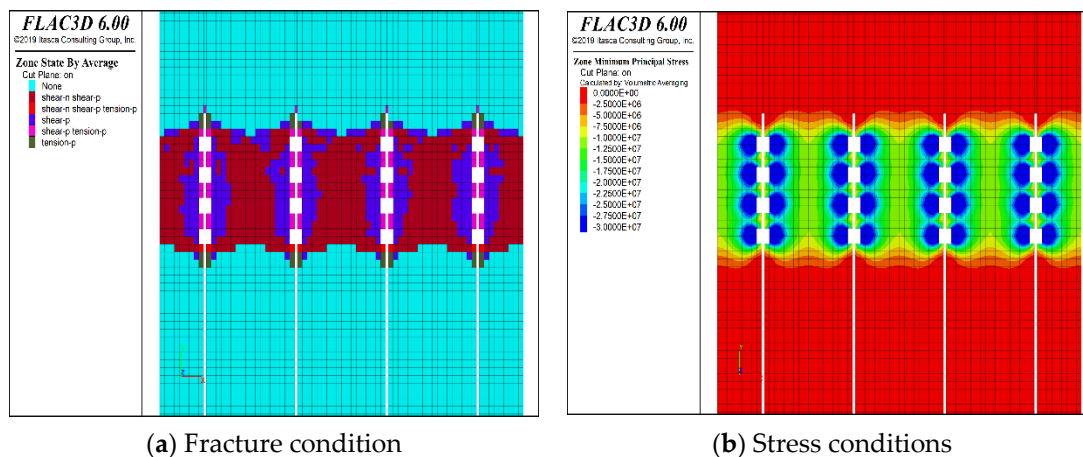
Figure 6. Simulation results of fracturing effect under designed hydraulic fracturing parameters.

4. In Situ Testing Results

The hydraulic fracturing of hard roofs included the following three main processes: borehole sealing, high-pressure water fracturing, and water pressure maintaining. Hydraulic fracturing boreholes 56 mm in diameter were arranged on the side of the coal body towards the working face, with the drilling direction opposite to the advancing direction of the working face. The spacing of the hydraulic fracturing boreholes was 7.0 m, and the angle between the boreholes and the roadway roof was 70°. The reverse fracturing method was used, which started from the bottom of the hydraulic fracturing borehole at fracturing intervals of 2.2 m. The fracturing layer of hydraulic fracturing was from the hole depth of 11.5 m to 21.6 m, with a total of four fracturing operations. The water injection pressure was designed to be 33 MPa, which was applied using the construction pump. Water pump pressure gauges are used to monitor the water injection pressure.

4.1. Hydraulic Fracturing Effect Analysis

During the fracturing process, the hydraulic fracturing situation of the working face was monitored. After the hydraulic fracturing was completed, a micro camera was used to observe the hydraulic fracturing boreholes. For the observation method, a borehole peeper was used to observe hydraulic fracturing boreholes inside the borehole. By observing the crack development shape of hydraulic fracturing boreholes, the crack development and expansion range of hydraulic fracturing boreholes were analyzed. The observed picture from one of the boreholes' hydraulic fracturing is shown in Figures 7 and 8. It was found that there were a large number of axial and radial cracks in the fracturing section of the hydraulic fracturing boreholes on the working face. The observed results indicated that the hydraulic fracturing parameters of the working face were reasonable, and the basic top-cut fractures were widely expanded, resulting in good hydraulic fracturing effects.

(**a**) At a depth of 14.0 m

(**b**) At a depth of 15.0 m

(**c**) At a depth of 17.0 m

(**d**) At a depth of 18.0 m
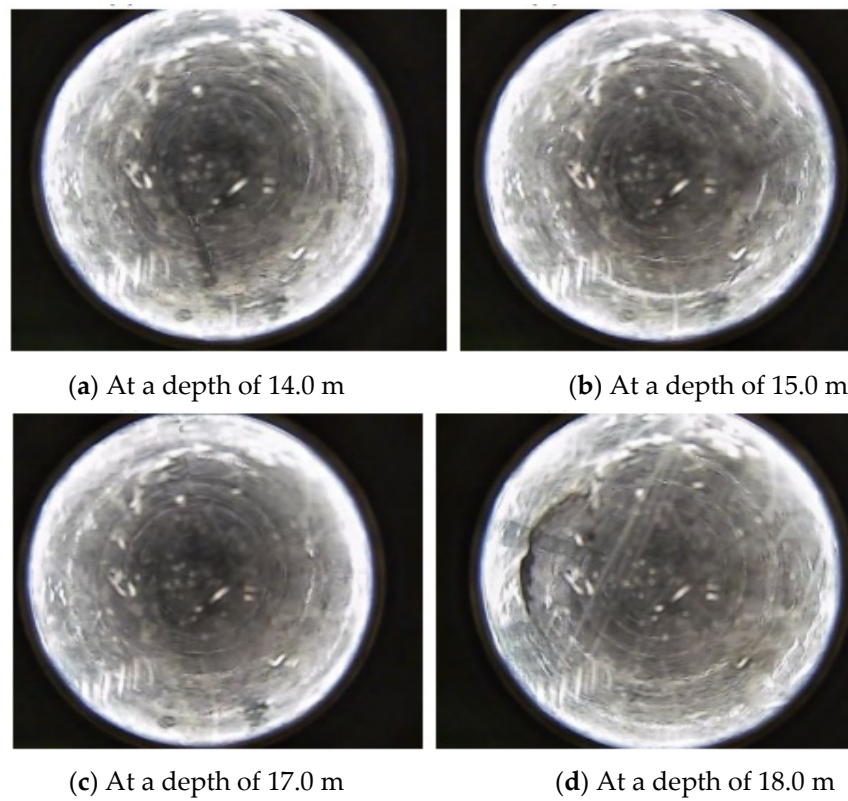
Figure 7. Hydraulic fracturing borehole observation results (transverse view).

(**a**) At a depth from 14.0 to 15.0 m

(**b**) At a depth from 15.0 to 16.0 m

(**c**) At a depth from 18.0 to 19.0 m

(**d**) At a depth from 19.0 to 20.0 m
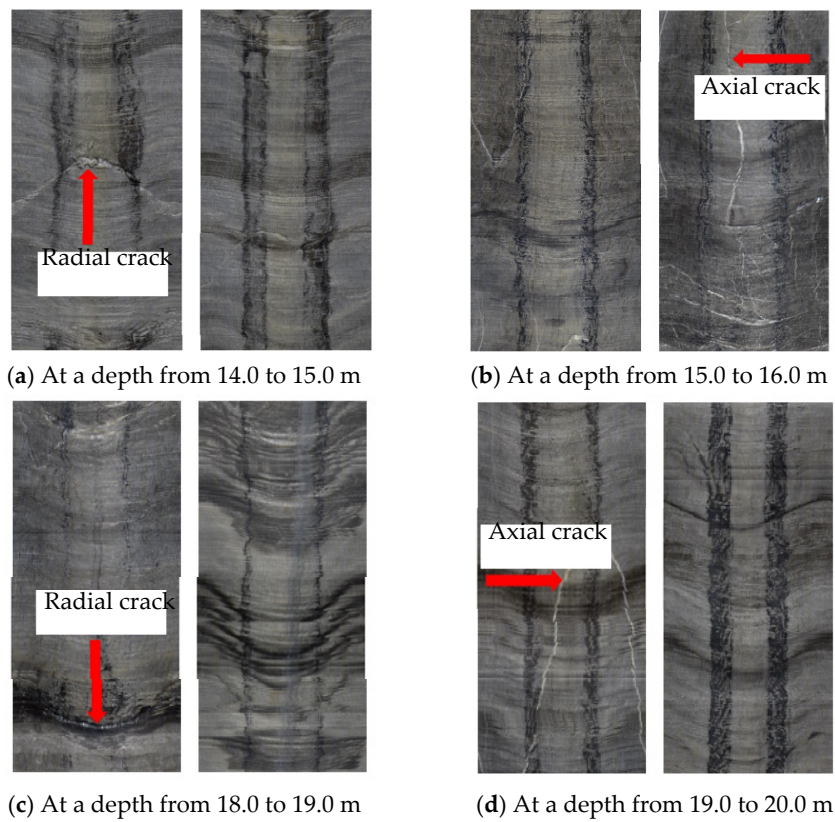
Figure 8. Hydraulic fractures in observed boreholes (longitudinal view).

4.2. Roadway Displacement and Pressure Analysis

To verify the effect of hydraulic fracturing on the hard roof of the working face, mining pressure monitoring points were arranged in the hydraulic fracturing section and the unfractured section of the return air roadway. The monitoring content included the displacement of the surrounding rock surface of the roadway and the vertical stress of the protective coal pillar. The cross-point method was used in conjunction with the top and bottom plate displacement and infrared rangefinder to monitor the top and bottom plate displacement and the two-sided displacement. The displacement sensors were installed at a distance of 15 m from the long-wall mining surface in the return air roadway. The deformation of the surrounding rock in the hydraulic fracturing section and the unfractured section were recorded for 100 days, with the results shown in Figure 9. According to the deformation monitoring results, it could be seen that the surface deformation of the roadway without hydraulic fracturing on the hard roof was basically stable after 80 days, the average displacement of the roadway top and bottom plate was 680.5 mm, and the average displacement of the two sides was 493.8 mm. For the hydraulic fractured section, the stability time of the surrounding rock was significantly earlier than that without hydraulic fracturing, and it tended to stabilize after 65 days. Compared to that without hydraulic fracturing, the surface deformation of the roadway's surrounding rock decreased, and the convergence speed of the roadway was significantly reduced. The displacement of the top and bottom plates decreased by 48.7%, and the displacement of the two sides decreased by 53.0%. This observation also indicated that the stress concentration around the roadway was eliminated, and pressure relief and stress transfer were realized, which also reduced the deformation of the roadway in the hydraulic fractured section.
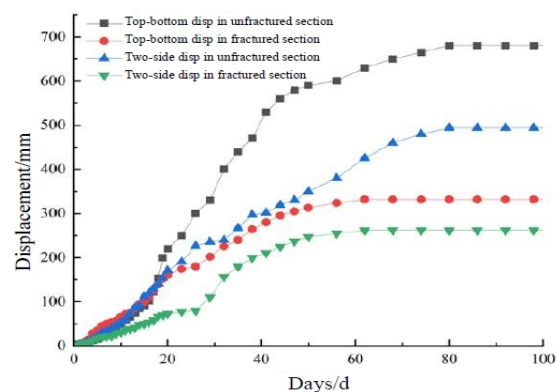
Figure 9. Surrounding rock deformation of return air roadway.

Four sets of borehole stress gauges were installed at a distance of 2.5 m from the surface of the coal pillar in the return air roadway, with a spacing of 2 m between each set of stress gauges. The continuous monitoring system was used to collect stress data from coal pillars. When the borehole stress gauge was located in the front of the working face, its distance from the working face was recorded as positive; when the borehole stress gauge was located behind the working face, its distance from the working face was recorded as negative. Coal pillar stress monitoring stopped when the working face advanced about 30 m past the monitoring point. The stress monitoring results of the coal pillar in the working face return air roadway are shown in Figure 10. Figure 10a shows the stress monitoring results of the coal pillar in the non-fractured section of the working face. It can be seen from the figure that when the borehole stress gauge was more than 50 m away from the working face, the vertical stress of the coal pillar increased slowly. As the distance from the working face decreased, the stress of the coal pillar increased significantly. When the working face advanced to the stress monitoring point, the stress growth rate of the coal pillar increased. Figure 10b shows the stress monitoring results of the coal pillar in the hard roof fracturing section of the working face. It can be seen that when the borehole stress gauge was more than 50 m away from the working face, the vertical stress of the coal pillar

changed slightly. However, as the distance from the working face decreased, the stress of the coal pillar gradually increased. When the working face advanced to 15 m behind the stress monitoring point, the stress of the coal pillar reached its peak due to the influence of the advanced support stress, and then the stress rapidly decreased. When it was 20 m behind the working face, it was basically stable.

(**a**) Non-fractured sections (**b**) Fractured sections
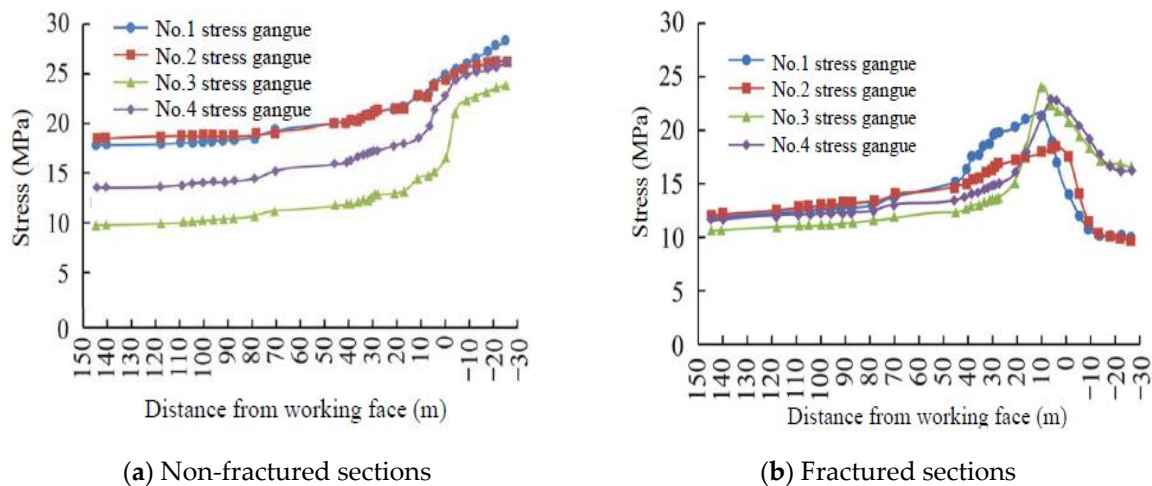
Figure 10. Stress monitoring of coal pillars in the return air roadway.

By comparing the monitoring results of coal pillar stress in the hydraulic fracturing section to that in the non-hydraulic fracturing section, it could be concluded that the peak point of the pillar stress in the non-hydraulic fracturing section appeared near 15 m of the working face. The difference in the peak stress location between the fracturing and non-fracturing sections was mainly caused by the hard roof weakening of hydraulic fracturing. The stress concentration around the roadway was eliminated. Pressure relief and stress transfer were realized, and the stress state of the roadway surrounding the rock was improved, which helped to control and maintain the roadway surrounding the rock.

5. Conclusions

The hydraulic fracturing effects on hard roofs under different hydraulic fracturing conditions were investigated through numerical simulation and in situ tests. The layout parameters of hydraulic fracturing for the hard roof of the working face were determined. The hydraulic fracture cutting and pressure relief principle of the hard roof of the working face was analyzed, and relevant parameters obtained from the analysis were used. The results showed that hydraulic fracturing parameters, including fracturing intervals, water injection pressures, and borehole spaces, all had direct effects on the efficiency of hydraulic fracturing. Based on designed hydraulic fracturing, industrial tests were conducted in the field while the stress and deformation were recorded. Compared to the hydraulic fracturing section, the peak point of the pillar stress in the non-hydraulic fracturing section appeared near 15 m of the working face, which indicated the effectiveness of hydraulic fracturing in weakening the hard roof and reducing the stress concentration. Hydraulic fracturing destroyed the cantilever beam structure above the small coal pillar in the working face, eliminated the stress concentration caused by the compression of the hard roof, and helped to maintain the roadway surrounding rock. The proposed methods and obtained results provided a theoretical and technical basis for the in situ hydraulic fracturing design of the hard roof of the working face in underground mines. Additionally, directional hydraulic fracturing, as well as the effects of the residual rock underground after coal mining, were needed to further study the treatment of hard roofs in coal mines.

Author Contributions: Methodology, S.W.; Validation, X.C.; Data curation, Q.H. All authors have read and agreed to the published version of the manuscript.

Data Availability Statement: The data presented in this study are available on request from the corresponding author.

Conflicts of Interest: The authors declare no conflict of interest.

References

1. He, Q.; Suorineni, F.T.; Oh, J. Strategies for Creating Prescribed Hydraulic Fractures in Cave Mining. *Rock Mech. Rock Eng.* **2017**, *50*, 967–993. [CrossRef]
2. Vu, T.T. Solutions to prevent face spall and roof falling in fully mechanized longwall at underground mines, Vietnam. *Min. Miner. Depos.* **2022**, *16*, 127–134. [CrossRef]
3. Lin, B.; Wang, Z.; Wang, R. Fracture extension and coal breaking performance by high-pressure gas-liquid jet flow. *J. China Univ. Min. Technol.* **2020**, *49*, 1–12.
4. Symanovych, H.; Odnovol, M.; Yakovenko, V.; Sachko, R.; Shaikhlislamova, I.; Reshetilova, T.; Stadnichuk, M. Assessing the geomechanical state of the main working network state in the case of undermining in the conditions of weak rocks. *Min. Miner. Depos.* **2023**, *17*, 91–98. [CrossRef]
5. Huang, B.; Wang, Y.; Cao, S. Cavability control by hydraulic fracturing for top coal caving in hard thick coal seams. *Int. J. Rock Mech. Min.* **2015**, *74*, 45–57. [CrossRef]
6. Wu, S.; Hao, W.; Yao, Y.; Li, D. Investigation into durability degradation and fracture of cable bolts through laboratorial tests and hydrogeochemical modelling in underground conditions. *Tunn. Undergr. Space Technol.* **2023**, *138*, 105198. [CrossRef]
7. Yang, W.; Lin, M.; Walton, G.; Lin, B.; Sinha, S.; Lu, C.; Li, G. Blasting-enhanced water injection for coal and gas out-burst control. *Process Saf. Environ. Prot.* **2020**, *140*, 233–243. [CrossRef]
8. Abe, A.; Kim, T.W.; Horne, R.N. Laboratory hydraulic stimulation experiments to investigate the interaction between newly formed and preexisting fractures. *Int. J. Rock Mech. Min.* **2021**, *141*, 104665. [CrossRef]
9. Xia, B.; Zhang, X.; Yu, B.; Jia, J. Weakening effects of hydraulic fracture in hard roof under the influence of stress arch. *Int. J. Min. Sci. Technol.* **2018**, *28*, 951–958. [CrossRef]
10. Zhang, F.; Wang, X.; Bai, J.; Wu, W.; Wu, B.; Wang, G. Fixed-length roof cutting with vertical hydraulic fracture based on the stress shadow effect: A case study. *Int. J. Min. Sci. Technol.* **2021**, *32*, 295–308. [CrossRef]
11. Wu, S.; Zhang, Z.R.; Chen, J.H.; Yao, Y.; Li, D.Q. Characterisation of stress corrosion durability and time-dependent performance of cable bolts in underground mine environments. *Eng. Fail. Anslysis* **2023**, *150*, 107292. [CrossRef]
12. Duan, M.; Jiang, C.; Gan, Q.; Li, M.; Peng, K.; Zhang, W. Experimental investigation on the permeability, acoustic emission and energy dissipation of coal under tiered cyclic unloading. *J. Nat. Gas Sci. Eng.* **2020**, *73*, 103054. [CrossRef]
13. Li, J.; Wu, T.; Lu, Z.; Wu, S. Investigation into Mining Economic Evaluation Approaches Based on the Rosenblueth Point Estimate Method. *Appl. Sci.* **2023**, *13*, 9011. [CrossRef]
14. Cheon, D.-S.; Lee, T.J. Theoretical Background and Design of Hydraulic Fracturing in Oil and Gas Production. *Tunn. Undergr. Space* **2013**, *23*, 538–546. [CrossRef]
15. Hubbert, M.K.; Willis, D.G. Mechanics of hydraulic fracturing. *Trans. AIME* **1957**, *210*, 153–168. [CrossRef]
16. Griffith, A. The phenomena of rupture and flows in solids. *Philos. Trans. R. Soc. Lond.* **1921**, *221*, 163–198.
17. Palaniswamy, K.; Knauss, W.G. On the Problem of Crack Extension in Brittle Solids under General Loading. *Mech. Today* **1978**, *4*, 87–148.
18. Fan, J.; Dou, L.; He, H.; Du, T.; Zhang, S.; Gui, B.; Sun, X. Directional hydraulic fracturing to control hard-roof rockburst in coal mines. *Int. J. Min. Sci. Technol.* **2012**, *22*, 177–181. [CrossRef]
19. Kanevskaya, R.D.; Diyashev, I.R.; Nekipelov, Y.K. Application of hydraulic fracturing for oil production stimulation and oil recovery increase. *Neft. Khozyaistvo* **2002**, *1*, 96–100.
20. Lu, G.; Gordeliy, E.; Prioul, R.; Aidagulov, G.; Bunger, A. Modeling simultaneous initiation and propagation of multiple hydraulic fractures under subcritical conditions. *Comput. Geotech.* **2018**, *104*, 196–206. [CrossRef]
21. Xing, Y.; Huang, B.; Li, B.; Liu, J.; Cai, Q.; Hou, M.; Liu, H. Investigations on the Directional Propagation of Hydraulic Fracture in Hard Roof of Mine: Utilizing a Set of Fractures and the Stress Disturbance of Hydraulic Fracture. *Lithosphere* **2021**, *2021*, 4328008. [CrossRef]
22. Zheng, K.; Zhang, T.; Zhao, J.; Liu, Y.; Yu, F. Evolution and management of thick-hard roof using goaf-based multistage hydraulic fracturing technology-A case study in western Chinese coal field. *Arab. J. Geosci.* **2021**, *14*, 876.
23. Zoveidavianpoor, M.; Samsuri, A.; Shadizadeh, S.R. Well Stimulation in Carbonate Reservoirs: The Needs and Superiority of Hydraulic Fracturing. *Energy Sources Part A Recovery Util. Environ. Eff.* **2013**, *35*, 92–98. [CrossRef]

24. Deng, J.Q.; Lin, C.; Yang, Q.; Liu, Y.R.; Tao, Z.F.; Duan, H.F. Investigation of directional hydraulic fracturing based on true tri-axial experiment and finite element modeling. *Comput. Geotech.* **2016**, *75*, 28–47. [CrossRef]
25. Ham, S.-M.; Kwon, T.-H. Characteristics of steady-state propagation of hydraulic fractures in ductile elastic and two-dimensionally confined plate media. *Int. J. Rock Mech. Min.* **2019**, *114*, 164–174. [CrossRef]
26. Ham, S.-M.; Kwon, T.-H. Video data of hydraulic fracture propagation in two-dimensionally confined gelatin plates. *Data Brief* **2019**, *25*, 104096. [CrossRef]
27. He, Q.; Suorineni, F.; Oh, J. Modeling interaction between natural fractures and hydraulic fractures in block cave mining. In Proceedings of the 49th US Rock Mechanics/Geomechanics Symposium, San Francisco, CA, USA, 28 June–1 July 2015.